



Magnesium hydroxide-incorporated PLGA composite attenuates inflammation and promotes BMP2-induced bone formation in spinal fusion

Tarek M. Bedair^{1,2*}, Chang Kyu Lee^{3*}, Da-Seul Kim^{1,4*} ,
Seung-Woon Baek^{1,5}, Hanan M. Bedair⁶, Hari Prasad Joshi⁷ ,
Un Yong Choi⁷, Keun-Hong Park¹, Wooram Park⁸, InBo Han⁷ and
Dong Keun Han¹ 

Abstract

Spinal fusion has become a common surgical technique to join two or more vertebrae to stabilize a damaged spine; however, the rate of pseudarthrosis (failure of fusion) is still high. To minimize pseudarthrosis, bone morphogenetic protein-2 (BMP2) has been approved for use in humans. In this study, we developed a poly(lactide-co-glycolide) (PLGA) composite incorporated with magnesium hydroxide (MH) nanoparticles for the delivery of BMP2. This study aimed to evaluate the effects of released BMP2 from BMP2-immobilized PLGA/MH composite scaffold in an in vitro test and an in vivo mice spinal fusion model. The PLGA/MH composite films were fabricated via solvent casting technique. The surface of the PLGA/MH composite scaffold was modified with polydopamine (PDA) to effectively immobilize BMP2 on the PLGA/MH composite scaffold. Analyzes of the scaffold revealed that using PLGA/MH-PDA improved hydrophilicity, degradation performance, neutralization effects, and increased BMP2 loading efficiency. In addition, releasing BMP2 from the PLGA/MH scaffold significantly promoted the proliferation and osteogenic differentiation of MC3T3-E1 cells. Furthermore, the pH neutralization effect significantly increased in MC3T3-E1 cells cultured on the BMP2-immobilized PLGA/MH scaffold. In our animal study, the PLGA/MH scaffold as a BMP2 carrier attenuates inflammatory responses and promotes BMP2-induced bone formation in posterolateral spinal fusion model. These results collectively demonstrate that the BMP2-immobilized PLGA/MH scaffold offers great potential in effectively inducing bone formation in spinal fusion surgery.

Keywords

Spinal fusion, osteogenesis, poly(lactide-co-glycolide), magnesium hydroxide, bone morphogenetic protein-2

Date received: 11 September 2020; accepted: 30 September 2020

¹Department of Biomedical Science, CHA University, Seongnam-si, Gyeonggi-do, Republic of Korea

²Chemistry Department, Faculty of Science, Minia University, El-Minia, Egypt

³Department of Neurosurgery, Keimyung University Dongsan Medical Center, Daegu, Republic of Korea

⁴School of Integrative Engineering, Chung-Ang University, Dongjak-gu, Seoul, Republic of Korea

⁵Department of Biomedical Engineering, Sungkyunkwan University, Jangan-gu, Gyeonggi-do, Republic of Korea

⁶Department of Clinical Pathology, National Liver Institute, Menoufia University, Menoufia, Egypt

⁷Department of Neurosurgery, CHA University School of Medicine, CHA Bundang Medical Center, Seongnam-si, Gyeonggi-do, Republic of Korea

⁸Department of Biomedical-Chemical Engineering, The Catholic University of Korea, Bucheon-Si, Gyeonggi-do, Republic of Korea

*These authors contributed equally to this work.

Corresponding authors:

Dong Keun Han, Department of Biomedical Science, CHA University, 335 Pangyo-ro, Bundang-gu, Seongnam-si, Gyeonggi-do 13488, Republic of Korea.

Email: dkhan@cha.ac.kr

InBo Han, Department of Neurosurgery, CHA University School of Medicine, CHA Bundang Medical Center, Seongnam-si, Gyeonggi-do 13496, Republic of Korea.

Email: hanib@cha.ac.kr



Introduction

Spinal fusion is a gold standard surgical intervention to connect two or more vertebrae to restore spinal stability in the treatment of various spinal diseases, including spinal stenosis, spinal instability, spinal fractures, and progressive scoliosis. Pseudarthrosis (failure of fusion) is a serious and challenging complication of spinal fusion surgery; it leads to severe pain and mobility impairment and the rate of pseudarthrosis following spinal fusion is reportedly as high as 48%.¹

To enhance the spinal fusion rate, spine surgeons have used various methods, including autologous bone graft materials, allogeneic bone graft materials (e.g. demineralized bone allograft), synthetic bone graft materials (e.g. tricalcium phosphate, hydroxyapatite, bioglass), and bone morphogenetic protein-2 (BMP2); each material has benefits and disadvantages.^{1–8} BMP2 was approved in 2002 and is currently used in spinal fusion surgery. Despite the effectiveness of BMP2 on osteogenic differentiation and bone formation, the delivery of BMP2 alone is not effective in assisting bone formation due to its short half-life. BMP2 experiences rapid diffusion throughout the body's fluids and thus quick clearance.⁷ Therefore, supraphysiological doses of BMP2 have been used clinically to promote bone formation; high doses of BMP2 have been associated with serious complications, including soft tissue inflammation and heterotopic ossification.^{9–11}

Therefore, given the rapid clearance of BMP2 from the body, substantial amounts of research have focused on developing more suitable biomaterials for BMP2 delivery. Many carriers and delivery systems comprised of different materials have been investigated to maintain the controlled release and improve the safety and therapeutic efficacy of BMP2.^{5,10–16} The delivery systems come in the form of hydrogels, microspheres, nanoparticles, and fibers. The carriers used for delivery are made of metals, ceramics, polymers, and composites.^{5,10–19}

Poly(lactic-co-glycolic acid) (PLGA) has been the most successful polymeric biomaterial for use in controlled drug delivery systems.^{16,18,20} Many PLGA delivery systems for BMP2 have shown promise for bone repair.^{21–26} However, the degradation of PLGA can decrease the pH in the surrounding tissues, causing inflammation or foreign body reactions *in vivo*.²⁷ Thus, many attempts have been made to reduce the inflammation and improve the biocompatibility of PLGA.^{21–26}

We have developed a composite scaffold composed of PLGA and magnesium hydroxide (MH, Mg(OH)₂) with a solvent casting method to reduce pH and inflammation. Following the pattern of previous reports, our PLGA/MH composite scaffold promoted a pH neutralization effect in the acidic microenvironments, an anti-inflammatory effect, and mechanical strength^{3,28–31} compared to the PLGA scaffold. We also confirmed the positive effect of the PLGA/Mg(OH)₂ scaffold on tissue regeneration through pH

neutralization of acids and anti-inflammation in a partially nephrectomized mouse model and a rat osteochondral defect model.^{31,32} Based on the finding from our previous studies, in this study, we designed a PLGA/MH composite scaffold with pH neutralization and anti-inflammatory properties on the implanting site.^{7,19,32–36} Additionally, in order to enhance osteogenic activity, the PLGA/MH composite scaffold surface was coated with polydopamine (PDA) as an adhesive interlayer and BMP2 was sequentially immobilized on the PDA-coated PLGA/MH composite scaffold. After configuring the scaffold, we evaluated *in vitro* and *in vivo* osteogenic activity of the BMP2-immobilized PLGA/MH scaffold. Our results indicate that this approach could be applied to mitigate the disadvantages of the materials currently available for spinal fusion and effectively enhance bone regeneration.

Materials and methods

Materials

Poly(lactic-co-glycolic acid) (PLGA, lactide/glycolide = 50:50, molecular weight 110 kDa) was obtained from Evonik Ind. (Essen, Germany). Magnesium hydroxide (MH), dopamine (DA), and tris(hydroxymethyl)aminomethane (Tris) were purchased from Sigma-Aldrich (Korea). Bovine serum albumin was purchased from MoreBio Co., Ltd and Pivotal Scientific (Korea). Phosphate-buffered saline (PBS) tablets were purchased from Gibco (Grand Island, NY, USA). Recombinant human bone morphogenetic protein-2 (rhBMP2) was obtained from CGBio Co., Ltd (Seongnam, Korea). The BMP2 ELISA kit was obtained from Antigenix America Inc. (New York, USA). The Micro BCA protein assay kit, Calcein AM, and ethidium homodimer-1 were purchased from Thermo Fisher Scientific (USA). A cell Counting Kit-8 (CCK-8) was purchased from Dojindo Molecular Technology, Inc. (USA).

Fabrication of the PLGA composite

The formation of PLGA film has been performed using a solvent casting method. In the beginning, 2 g of PLGA were dissolved in 8 g of chloroform under rolling using desktop ball mill (LM-BD6030, LK lab, Namyangju-si, Korea) for 4 h. Next, the solution was carefully poured into a Teflon mold. The solvent was allowed to evaporate slowly for 2 days at room temperature. The PLGA film that formed was further dried under vacuum at room temperature for 1 day, and then it was cut into 3 × 7 mm sections for *in vitro* and *in vivo* experiments.

Fabrication of the PLGA/MH composite

The PLGA/MH films were prepared using the same protocol for PLGA film preparation. Briefly, 1.7 g of PLGA and

0.3 g of MH nanoparticles were dissolved in 8 g of chloroform followed by bath sonication for 30 min. Thereafter, it was rolled for 4 h until a homogenous solution was obtained. The remaining protocol was similar to the standard for PLGA film and the resulting film was coded as PLGA/MH.

Polydopamine coating on the PLGA and PLGA/MH composites

For all PLGA and PLGA/MH films, 250 μ L of the prepared dopamine solution (2 mg of dopamine, and 1 ml of Tris solution (10 mM, pH 8.5) were used to coat polymer film at room temperature for 4 h under shaking conditions. The films were sonicated in water for 5 min in low mode, followed by washing in deionized water three times. These steps were repeated one more time to obtain films with a homogenous coating of PDA. The prepared films were coded as PLGA-PDA and PLGA/MH-PDA films, respectively.

BMP2 immobilization on the PLGA-PDA and PLGA/MH-PDA composites

The PLGA-PDA and PLGA/MH-PDA films were sterilized in ethanol and under UV light, then immersed in TRIS/BMP2 solution and allowed to react for 24 h at 37°C under 100 rpm shaking conditions. The BMP2 immobilized films were immersed in sterilized deionized water to remove the physically and loosely bound BMP2. For in vitro analysis, the films were dried under vacuum at room temperature, whereas for in vitro cells and in vivo experiments, the samples were immersed in sterilized PBS solution and implanted directly into mice.

Characterizations of the PLGA/MH composite

Surface characterization. Attenuated total reflectance-Fourier transform infrared spectroscopy (ATR-FTIR, FT/IR-4100, Jasco Analytical Instruments, USA) was used to determine the chemical bonds and the functional groups present in the control PLGA and PLGA composites. Surface wettability of PLGA film was determined using contact angle goniometry (DGD Fast/60 Contact Angle Meter, Phoenix, AZ, USA). A droplet of deionized water (2 μ L) was carefully dropped on the surface for 45 s and the average of six readings was calculated from three different films. The change in surface morphology of the surface was confirmed by field emission-scanning electron microscopy (FE-SEM, S-4100, Hitachi, Japan). The surfaces of the samples were sputtered with platinum under an argon atmosphere for 60 s before observation.

Thermal property. The amount of MH in the PLGA matrix and the thermal stability were investigated by thermogravimetric analysis (TGA, TGA 4000 instrument,

PerkinElmer, USA). Approximately, 8 mg of polymer film was heated from room temperature to 800°C at a heating rate of 10°C/min with a nitrogen flow of 19.8 mL/min. The amount of inorganic MH content was recorded from the mass change *versus* temperature curve.

Degradation behavior and pH study. Control PLGA and PLGA/MH composites were placed in vials containing 1 ml of PBS solution in a shaking water bath under physiological conditions (pH 7.4, 100 rpm and 37°C). At predetermined time points (1, 3, 5, 7, 14, 21, 28, 35, 42, 49, and 56 days), pH level was determined via pH-meter (Mettler Toledo, Ohio, USA). For the residual mass percentage determination, the film was cut (3 \times 7 mm), initially weighted (W_0), immersed in PBS solution for a predetermined time, washed by deionized water, dried under vacuum for 2 days, and finally weighed (W_t). The residual weight percentage was calculated from the following equation:

$$\text{Residual weight percentage (\%)} = \left((W_0 - W_t) / W_0 \right) \times 100$$

Quantification of the amounts of residual polydopamine on the composites. The amounts of residual PDA on the surfaces of the PLGA and PLGA/MH composites were determined through Micro BCA assay. In short, the coated films were immersed in 500 μ L of Micro BCA solution and 500 μ L of deionized water for 2 h at 37°C. Thereafter, 200 μ L of the violet color was transferred to non-tissue culture 96 well plate for UV absorbance at 562 nm. A standard curve was obtained through a series of standard dopamine solution.

BMP2 quantification using ELISA method. The amount of BMP2 onto the surface of polymer films, was determined by using an indirect method, in which the initial and the unreacted BMP2 was measured using the ELISA kit, and the UV absorbance was recorded at 450 nm. The load of BMP2 was calculated by subtracting the amount of unreacted BMP2 from the initial amount. The BMP2 loaded onto control PLGA and PLGA/MH composites was immersed in 4 M Guanidine-HCl and protease inhibitors. It followed the assay procedure and at predetermined time (1, 3, 5, 7, 14, 21, 28, 35, 42, 49, and 56 days), the amount of released BMP2 was determined.

In vitro cell study

Cell culture. The osteoblast precursor cells (MC3T3-E1) were cultured in a humidified atmosphere incubator at 37°C with 5% CO₂. The cells were grown in a T25 tissue culture flask containing 7 mL of α -MEM containing 10% fetal bovine serum and 1% antibiotic-antimycotic solution. The culture medium was changed every other day until the cells reached 85% confluence. The cells were then detached with trypsin/EDTA solution. After centrifugation

at 1300 rpm for 3 min, the cells were suspended in α -MEM with a concentration of 1×10^4 cells/mL.

Cell attachment study. The PLGA and PLGA/MH composites were placed in 24-well culture plates and sterilized with 70% alcohol for 3 h. The cell suspensions at densities of 2.5×10^4 cells/mL were seeded in the wells. After 4 h, the films were washed with PBS solution followed by CCK-8 assay. Briefly, 400 μ L of 10% CCK-8 solution was added to the well. After incubating the samples for 3 h, 100 μ L of solution was transferred to a 96-well for UV measurements at 450 nm using a microplate reader (SpectraMax M2, Molecular Devices, San Jose, USA).

Cell proliferation assay. The sterilized films were dipped in a cell suspension of 1×10^4 cells/mL. The proliferation study of MC3T3-E1 cells was evaluated using a CCK-8 assay at days 1, 3, and 7. Briefly, after day 1, the films were transferred to new non-treated 24-well culture plates, washed with 500 μ L of fresh media, and a CCK-8 assay was performed as outline above. The proliferated cells were stained using live/dead staining kits as previously reported.³⁷

Osteoblast differentiation

Alkaline phosphatase (ALP) staining. The cells were cultured on each film for 1 day before treatment with osteogenic differentiation medium. After allowing 1 day for cell adhesion to take place, osteogenic differentiation medium (10 mM β -glycerophosphate, 50 μ g/ml ascorbic acid, and 100 nM dexamethasone in growth medium) were added to the cell culture film for 21 days. The ALP staining was performed with Takara TRACP&ALP double-stain kit following the manufacturer's protocol (Takara Bio, Kyoto, Japan).

Gene expression analysis. Quantitative real-time reverse transcription polymerase chain reaction (qRT-PCR) was used to quantify the bone related mRNA expression levels of GAPDH, alkaline phosphatase (ALP), osteocalcin (OCN), and runt-related transcription factor 2 (RUNX2). Total RNA from the cultured cells was extracted using AccuPrep universal RNA extraction kit (Bioneer, Daejeon, Korea) following the manufacturer's protocol. The RNA concentration was determined by spectrophotometry (ND-1000, NanoDrop; Thermo Fisher Scientific, Massachusetts, USA). RNA was reverse-transcribed using a PrimeScript™ RT Reagent Kit (Perfect Real Time) to cDNA in triplicate for each sample. PCR was performed using Power SYBR Green PCR Master Mix (Applied Biosystems, California, USA) with a QuantStudio 3 real-time PCR instrument (Applied Biosystems, California, USA). The primer sequences related to osteogenic differentiation are shown in Supplemental Table S1.

Animal response to BMP2-immobilized PLGA/MH scaffolds

Animal grouping and surgery. All the animal experiments were performed under the approval of the Institutional Animal Care and Use Committee of CHA University. Ten-week old male C57BL/6 mice weighing 20 g were purchased from Orient Bio, Inc. (Seongnam, Korea) and were raised at 55–65% humidity and a controlled temperature of $24 \pm 3^\circ\text{C}$ with a light/dark cycle of 12 h. Animals were randomly divided into five groups: Group 1 received decortication-only ($n=7$), group 2 received PLGA films bilaterally ($n=10$), group 3 received PLGA/MH films bilaterally ($n=10$), group 4 received PLGA/BMP2 films bilaterally ($n=10$), and group 5 received PLGA/MH/BMP2 films bilaterally ($n=10$) (BMP2 dose; 0.3 μ g/film).

Surgical procedures. Mice were anesthetized with Zoletil (50 mg/kg; Virbac Laboratories, France)/Rompun (10 mg/kg; Bayer, Korea) solution administered intraperitoneally. Skin and hair covering the surgical site was shaved with a blade once mice were anesthetized, and the surgical site was prepped with povidone-iodine and 70% ethanol. Animals were positioned prone with folded gauze beneath the abdomen, increasing the excursion of the lumbar spine to facilitate access to and visibility of the surgical field. Aseptic technique was used for all surgical procedures. Posterolateral lumbar fusion at L4–6 was performed. Briefly, a 20 mm midline skin incision was performed through the skin and subcutaneous tissue over L4–6 down to the lumbar paravertebral fascia along the spinous processes. The lumbar paravertebral muscles overlaying the articular processes of L4–6 were separated from the spinous processes by scraping with a #10 blade. After exposing the articular processes, a pneumatic 1 mm diamond burr was used to decorticate the articular processes. We fabricated PLGA and PLGA/MH films through solvent casting and finally cut into (width: 3 mm, length: 7 mm). Films, two pieces of PLGA (3 mm [W] \times 7 mm [L] \times 0.5 mm [H]) contained with MH or BMP2 (0.3 μ g/film), were implanted over the bilateral decorticated articular processes on each site. The fascia and skin were closed layer by layer with 6–0 Vicryl. Mice were placed on a heating pad following surgery and monitored for recovery. Antibiotics were administered via drinking water for 24 h postoperatively. All mice were euthanized using carbon dioxide inhalation 4 weeks after implantation, and their spines were excised for evaluations.

Micro-computed tomography (CT)-based bone analysis. All the spinal samples were sacrificed at 4 weeks after implantation and scanned by Skyscan 1173 micro-CT machine (Skyscan, Kontich, Belgium). For bone histomorphometry, the new bone mass was isolated from native bone by means of a manually drawn region of interest (ROI). To quantify the density of bone formed within each new mass,

percent bone volume (BV) (BV/TV (the total volume of the mass)), bone mineral density (BMD), and trabecular thickness (Tb.thick, mm) were calculated.

Histology and immunohistochemistry. After micro-CT scanning, the spine samples were decalcified using decalcification solution (National Diagnostics, Atlanta, GA), the tissues were dehydrated by placing them in a graded series of ethanol and xylene and were finally embedded in paraffin; the axial sections (4 μm thickness) were obtained. The sections were stained with hematoxylin and eosin (H&E, Sigma-Aldrich, St. Louis, MO) and Masson's trichrome (Sigma-Aldrich, St. Louis, MO) to demonstrate new bone formation. For immunohistochemistry, the sections were incubated for 10 min at room temperature. Primary antibodies to osteocalcin (Santa Cruz Biotechnology, CA) and IL-6 (Santa Cruz Biotechnology, CA) were used, and biotin-conjugated anti-IgG secondary antibody was used.

Statistical analysis

The results were expressed as mean \pm standard deviation and statistically examined using one-way ANOVA following Tukey's post-hoc analysis using GraphPad Prism software (version 8). The results considered insignificant when $p > 0.05$ and statistically significance when $*p < 0.05$, $**p < 0.01$, and $***p < 0.001$.

Results and discussion

Surface modifications and characterizations

We fabricated a novel biodegradable anti-inflammatory polymeric composite for bone regeneration. Supplemental Figure S1 represents the schematic illustrations of the BMP2 immobilization on the surface of PLGA and PLGA/MH film with detailed process of BMP2 immobilization via PDA interlayer. Initially, PLGA was mixed with MH to enhance mechanical strength and reduce the inflammation due to the acidic microenvironment of polymer degradation. The surface of the composite scaffold was further modified with PDA to facilitate immobilization of BMP2 and to promote osteogenesis.³⁸

Figure 1(a) shows SEM images of the PLGA, PLGA/BMP2, PLGA/MH, and PLGA/MH/BMP2 films, respectively. The control PLGA film showed smooth and uniform surface; PLGA/MH composite also displayed a smooth and uniform surface. However, PLGA/BMP2 film and PLGA/MH/BMP2 film exhibited rough surfaces due to the PDA grafting and presence of BMP2 molecules. These composites experienced a slight loss of MH nanoparticles from the surfaces of the films during BMP2 immobilization. When compared with PLGA/BMP2 film, PLGA/MH/BMP2 film showed more roughness and some holes on the surface due to the partial loss of MH

particles during PDA coating and BMP2 immobilization (Figure 1(a)). Figure 1(b) shows the wide scan (650–4000 cm^{-1}), and narrow scan (650–2000 cm^{-1}) of ATR-FTIR spectra of the PLGA, PLGA/MH, PLGA/BMP2, and PLGA/MH/BMP2 films, respectively. FTIR is a technique commonly used to characterize the functional groups of coatings and film with a depth of up to 5 μm .^{37,39} For all of the films, several characteristic peaks were observed at 2950, 2850, 1755, 1453, 1380, and 1040 cm^{-1} , which are attributed to aliphatic C–H asymmetric, C–H symmetric stretching, O=C=O stretching, $-\text{CH}_2$ bending, $-\text{CH}_3$ bending, and C–CH₃ stretching vibrations, respectively. Moreover, two absorption peaks occurred at 1270 and 1085 cm^{-1} , which represent C–O–C stretching vibrations.³⁵ These peaks represent the characteristic peaks of PLGA structure as previously reported.⁴⁰ Interestingly, after the incorporation of MH nanoparticles, a new peak was observed at 3698 cm^{-1} , which is attributed to Mg–OH stretching.³⁵ After PDA coating and BMP2 immobilization, two new peaks were observed at 3505 and 1610 cm^{-1} , which represent N–H and C=C stretching vibrations, respectively.⁴¹ TGA analysis demonstrated that MH nanoparticles were incorporated on the film surface. Due to the MH presence, PLGA/MH and PLGA/MH/BMP2 demonstrate decrease in weight at 400 to 500°C (Figure 1(c)). Figure 1(d) shows water contact angle images of each films and measurements. The water contact angle measures the wettability of the surface, which could have a hydrophobic or hydrophilic property based on the physicochemical properties of the surface coating. A hydrophilic surface plays a crucial role, in both cell interactions and protein adsorption. This facilitates the incorporation of growth factors including fibronectin, and vitronectin; a hydrophobic surface does not exhibit the same incorporation tendencies.^{42,43} Compared to PLGA, the PLGA/MH composite film possessed more hydrophilic characteristics on its surface; its water contact angle was reduced from 94.6 to 87.6° due to the presence of surface MH. MH is a basic hydrophilic ceramic that could improve the hydrophilicity of polymer composites.³² After the modification of PLGA and PLGA/MH films with a thin layer of PDA, the wettability of the surface was improved with water contact angles of 66 and 48.6°, respectively.^{44,45} This change could be due to the amino groups present in the PDA structure on the surface. The water contact angle measurements are close to the theoretical value of a film containing purely PDA.^{45,46} After further modification of PLGA and PLGA/MH films with BMP2, the film demonstrated greater hydrophilicity with water contact angles of 55.5 and 44.4°, respectively.^{38,44} The higher hydrophilicity of the PLGA/MH/BMP2 sample could come from the presence of MH and hydrophilic BMP2 molecules on the surface, and furthermore its increased roughness value as compared to PLGA/BMP2 film could explain the difference.³⁸ The optimum range

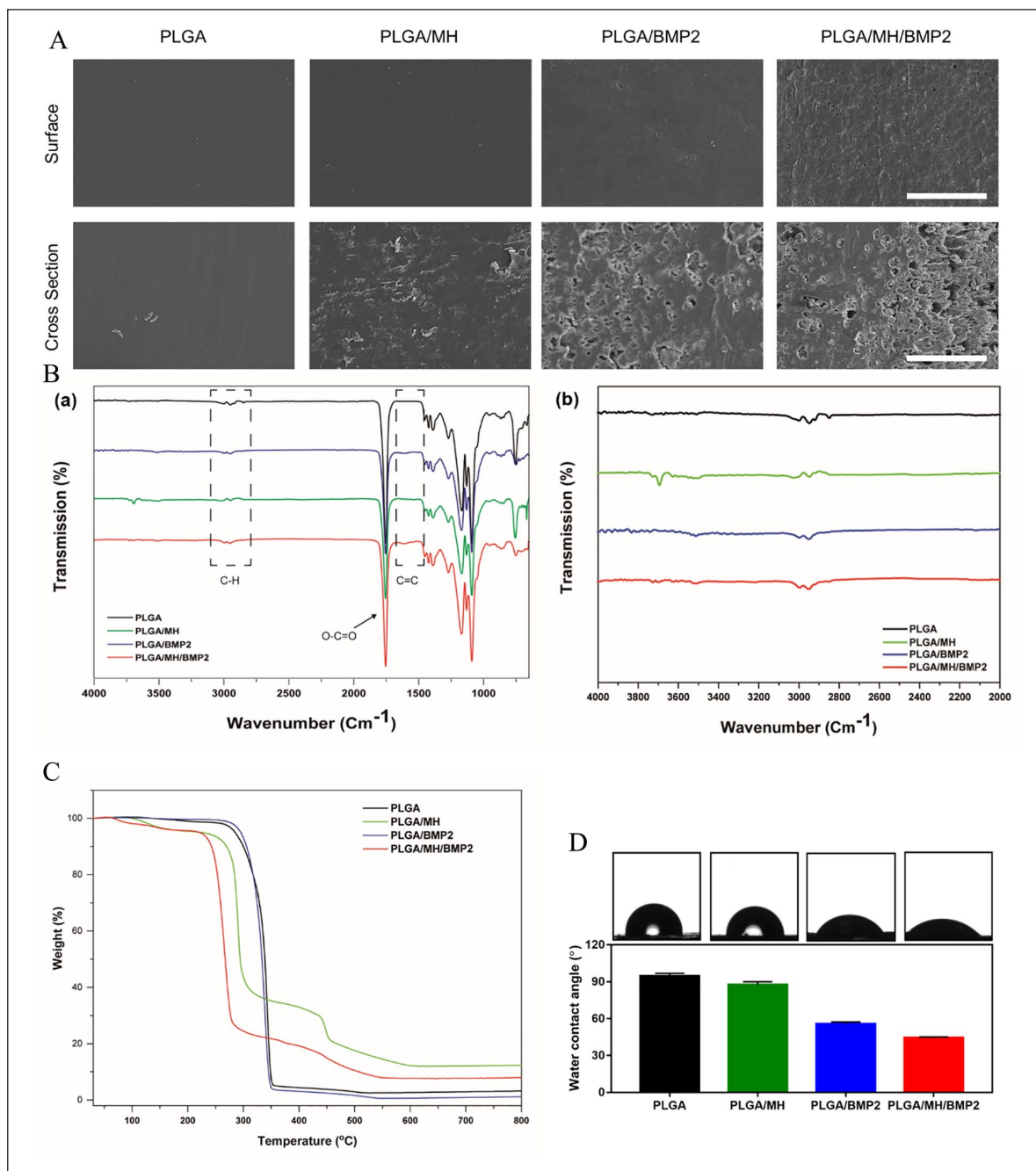


Figure 1. Surface modification and characterization of the PLGA films. (a) SEM images of surface and cross section of PLGA, PLGA/BMP2, PLGA/MH, and PLGA/MH/BMP2. Scale bar = 100 μm . (b) FTIR wide scan (650–4000 cm^{-1}) and narrow scan (2000–4000 cm^{-1}) spectra. (c) TGA thermograms for each film (37–800 $^{\circ}\text{C}$). (d) The water contact angle images of each films and measurements.

for cell adhesion on the culture substrate comes at a water contact angle of between 5 and 40 $^{\circ}$.^{38,47,48} This result shows that the PLGA/MH/BMP2 combination can provide the optimum microenvironment for cell attachment and proliferation.³⁸

Supplemental Figure S2 demonstrates the time dependent polymerization of PDA on the surface of PLGA and

PLGA/MH films. During the first 3 h, there are no significant differences in the amount of PDA on PLGA and PLGA/MH films. After 4 h of grafting, however, the PLGA/MH films show greater PDA coating as compared to PLGA (** $p < 0.001$). This might be a function of the rougher nature and higher hydrophilicity value of PLGA/MH film as compared to PLGA film. Moreover, the release

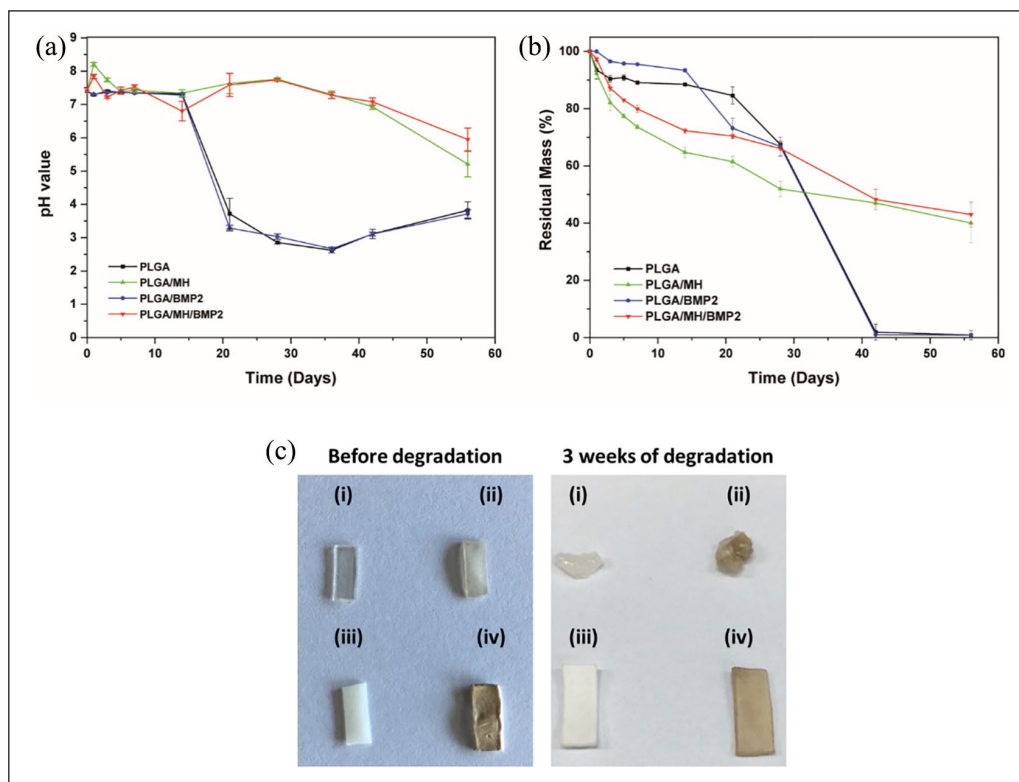


Figure 2. (a) The change of pH value and (b) percentage of residual weight (%) during degradation in PBS solution at physiological conditions (pH 7.4, 37°C, 100rpm). (c) The optical images of (i) PLGA, (ii) PLGA/BMP2, (iii) PLGA/MH, and (iv) PLGA/MH/BMP2 films before and after degradation for 3 weeks under physiological conditions (PBS solution, pH=7.4, 100 rpm, and 37°C).

of MH during the polymerization increased the pH value, which in turn accelerated the PDA polymerization, and consequently the amount of coating that was able to take place. In addition, the existence of magnesium cation on the surface could chelate with the catechol group of PDA and therefore increase the coating amount.⁴⁹ The optical images indicated different colors between PLGA and PLGA/MH before and after the PDA coating. Before coating with PDA, the control PLGA film displayed a colorless film, whereas the PLGA/MH composite film showed a white color. After PDA coating, the color became deep and dark with time, which denoted the presence of more PDA coating based on previous findings using Micro BCA. Moreover, the PDA-coated PLGA/MH films exhibited darker colors than the PDA-coated PLGA films.

Change of pH value and percentage of residual weight during degradation

The degradation of PLGA was took place under physiological conditions (100rpm, pH 7.4, 37°C) for up to 8 weeks. Figure 2(a) represents the change in pH seen during the degradation of PLGA and PLGA/MH composites. In the first 2 weeks, the PLGA films did not show any change in pH value, whereas at 3 weeks, the pH of PLGA dropped significantly to 3.7 and 3.2 for PLGA and PLGA/BMP2,

respectively, which was close to the pH values of lactic acid and glycolic acid.³¹ This phenomenon of PLGA degradation with acidic byproducts was duplicated across of several other publications.^{4,30,50} By contrast, the MH-incorporated PLGA samples showed a pH neutralization effect at a pH value slightly higher than physiological pH due to the release of basic MH ions; both PLGA/MH and PLGA/MH/BMP2 samples finally decreased to pH levels of 5.2 and 5.9 with mild acidity at 8 weeks, respectively. The weight changes seen during degradation of the control PLGA and PLGA/MH composites were significantly different as shown in Figure 2(b). Initially, the PLGA/MH composites showed rapid weight loss until the 21st day as compared to PLGA films, which might be due to the release of MH from the surface. At 42 days, PLGA films showed weight loss up to 98% to 99%, whereas the PLGA/MH composites displayed 52% to 53% weight loss. This sudden loss of weight at day 42 could have been the result of the self-backbiting mechanism of the PLGA film's under acidic environment.

Figure 2(c) shows the optical images before and after degradation of (i) PLGA, (ii) PLGA/BMP2, (iii) PLGA/MH, and (iv) PLGA/MH/BMP2 under physiological conditions. It was clear that after 3 weeks of degradation, PLGA and PLGA/BMP2 lost their shape and formed a gel-like structure. By contrast, PLGA/MH and PLGA/MH/BMP2 retained shapes similar to the originals; they were

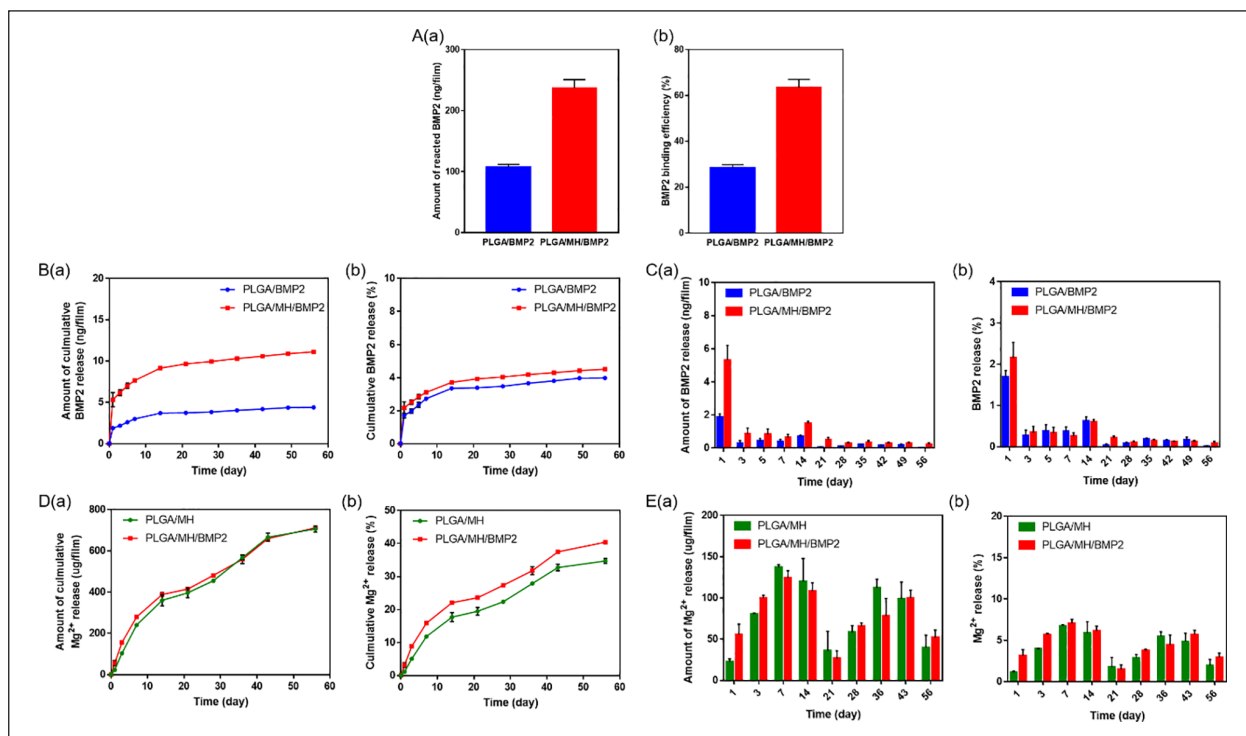


Figure 3. (a) BMP2 binding amount (ng/film) and BMP2 binding efficiency (%). (b) Cumulative BMP2 release and percentage of BMP2 release. (c) Amount of BMP2 released between every successive time points and percentage of BMP2 released between every successive time points for PLGA and PLGA/MH films. (d) and (e) Mg²⁺ release from PLGA/MH and PLGA/MH/BMP2 films (Film size: 3 mm × 7 mm, n = 3, ***p < 0.001).

only slightly longer and wider, which could be due to water uptake encouraged by MH nanoparticles.

Loading efficiency of BMP2 and release of BMP2 and MH

Figure 3 shows the efficiency and the total amount of grafted BMP2 onto the surfaces of PDA-coated PLGA and PLGA/MH films. It was clearly observed that the PLGA/MH film retained approximately 2.2 times more grafted BMP2 (237.4 ng) than the PLGA film (107.1 ng) (Figure 3(a)–(c)). These results demonstrate that PDA-coated PLGA/MH film bound BMP2 with more efficiently (63.4%) as compared to PDA-coated PLGA films (28.6%) (Figure 3(b)). This could be attributed to the more significant PDA surface coating on PLGA/MH film compared to control PLGA film (Supplemental Figure S2).³⁸ As mentioned previously, many approaches are available to overcome the disadvantages of BMP2 and improve both its safety and therapeutic efficacy by utilizing different carrier systems.^{5,10–16,38} The release profile of BMP2 from PLGA/BMP2 and PLGA/MH/BMP2 exhibited an initial burst release followed by slow release for up to 8 weeks (Figure 3(b) and (c)). Interestingly, the PLGA/MH/BMP2 film indicated a more significant release of BMP2 when compared to PLGA/BMP2 film. Figure 3(d) and (e) represents

the Mg²⁺ release profile during degradation for up to 8 weeks under physiological conditions. From the release profile, it was determined that both MH-containing films follow a sustained release profile without initial bursts. The BMP2 immobilized film released MH faster than the control PLGA/MH film. The improved hydrophilicity of the PLGA/MH/BMP2 film (40°) compared to PLGA/MH film (85°) might be responsible for this differential release.

In vitro biocompatibility

Figure 4(a) shows the viability of MC3T3-E1 cells on the PLGA, PLGA/MH, PLGA/BMP2, and PLGA/MH/BMP2 films for up to 7 days. At day 1, cell attachment was lower on the PLGA/BMP2 sample compared to other groups due to the better hydrophilicity of MH-polymer composites. On day 7, the proliferation of the cells on PLGA/MH/BMP2 significantly (***) increased compared to control PLGA along with the proliferation of the cells on PLGA/MH (*p < 0.05). Due to MH nanoparticles, PLGA/MH and PLGA/MH/BMP2 groups resist pH change from acidic PLGA byproducts. The Calcein AM stained images of MC3T3-E1 showed more live cells on the PLGA/MH and PLGA/MH/BMP2 surface compared to other samples, which indicates improved cell compatibility.

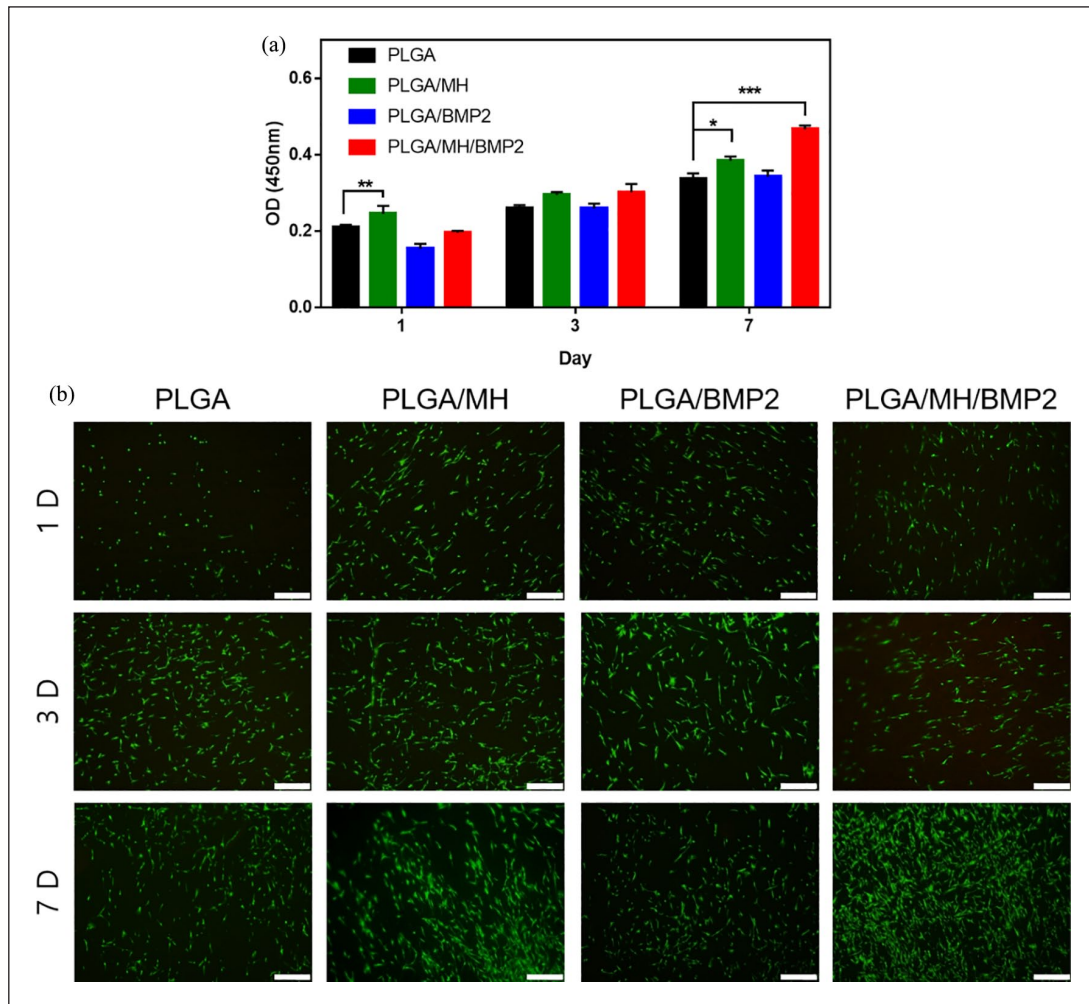


Figure 4. In vitro biocompatibility of each PLGA films. (a) Cell viability test using CCK-8 for 1, 3, and 7 days (* $p < 0.05$, ** $p < 0.01$, and *** $p < 0.001$). (b) Calcein AM staining for live cells on each film. Scale bar = 500 μm .

In vitro effect on osteogenic differentiation of osteoblast precursor cells

Based on the characterization of PLGA/MH/BMP2 (Figure 3), we hypothesized that the BMP2-immobilized films could accelerate osteogenic differentiation of osteoblast precursor cells. The MC3T3-E1 (murine calvarial cell line) cells were cultured on PLGA, PLGA/MH, PLGA/BMP2, and PLGA/MH/BMP2 films, and treated with a medium containing typical osteogenic differentiation factors, β -glycerophosphate, ascorbic acid and dexamethasone. In Figure 5, as mentioned previously, the BMP2-immobilized composite scaffold displayed the same significant differentiation seen in multiple studies prior to this one.^{2,9,19,25,38} Figure 5(a) contains the ALP stained images of each films after 7 days of osteogenic induction. The largest ALP stained area was found on the PLGA/MH/BMP2 film. To confirm the osteogenic differentiation, the mRNA expression levels of the two

pre-osteogenic markers (ALP and RUNX2) and the mature osteoblastic marker (OCN) were quantified by RT-qPCR. Figure 5(b) shows that the expressions of all three markers on PLGA/MH/BMP2 were significantly higher than what was seen on the other three films after 21 days of differentiation.

Bony fusion in animal studies

After 4 weeks of implantation, bony fusion between the L4 and L6 and new bone formation were determined by micro-CT analysis. New bone formation was not found in the decortication-only group and the PLGA-implanted group (group 2). Although the PLGA/MH-implanted group (group 3) showed no significant new bone formation, slightly increased new bone mass was found compared to groups 1 and 2, demonstrating that MH may enhance osteoblast activity temporarily.⁵¹ A large volume of new bone was observed in PLGA/BMP2 (group 4) and

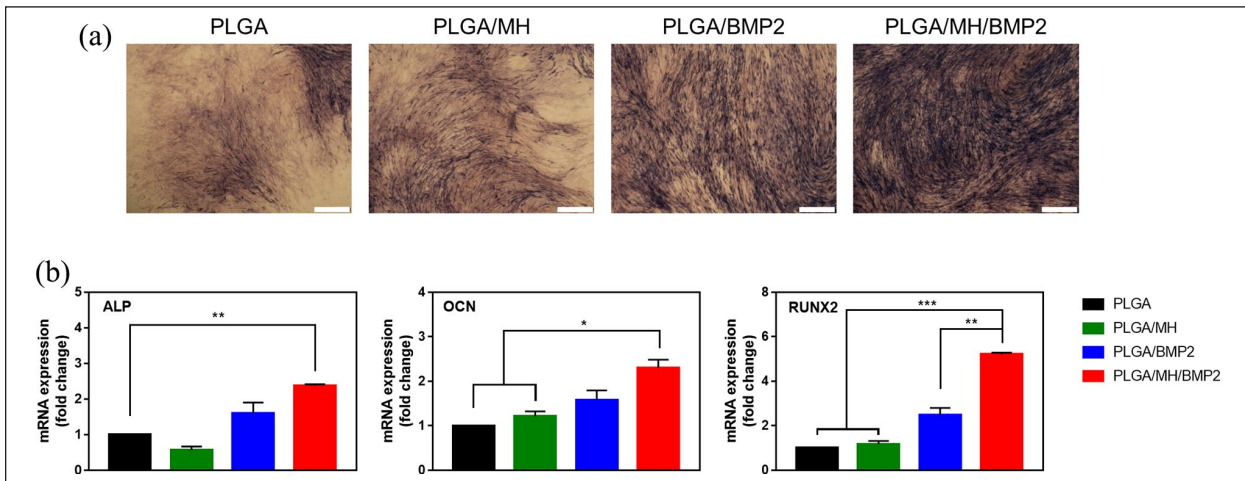


Figure 5. MT3T3-E1 cell differentiation on each PLGA films. (a) ALP stained images for 7 days. (b) The mRNA expression of ALP, OCN, and RUNX2 was determined by qPCR for 21 days (* $p < 0.05$, ** $p < 0.01$, and *** $p < 0.001$).

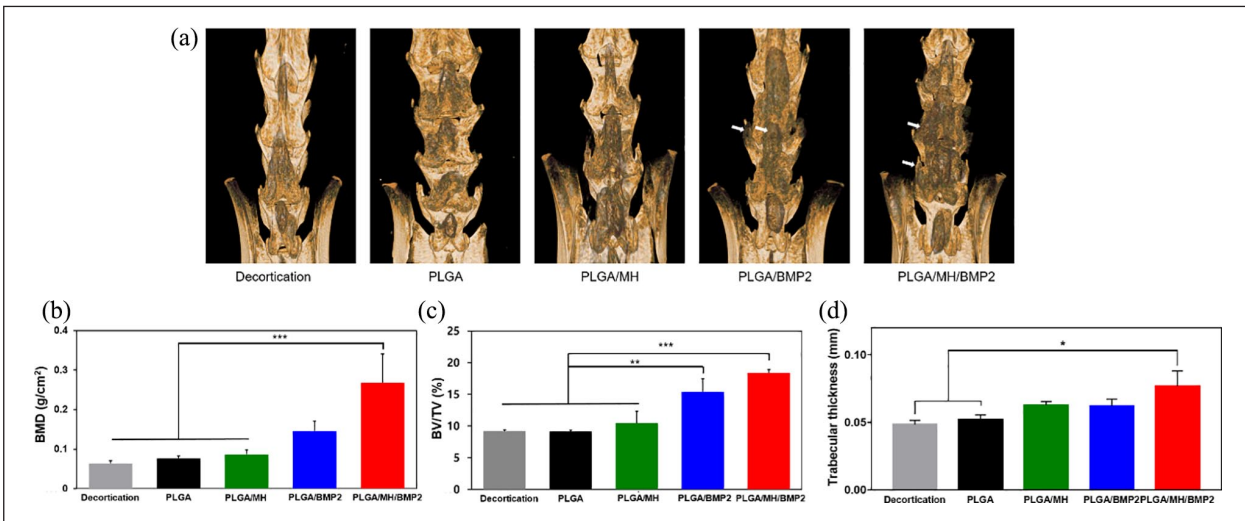


Figure 6. Micro-CT analysis of the L4-6 fusion mass. (a) Representative 3D micro-CT images of the fusion mass. (b) Bone histomorphometry showing bone mineral density (BMD), bone volume fraction (BV/TV), and trabecular thickness (* $p < 0.05$, ** $p < 0.01$, and *** $p < 0.001$).

PLGA/MH/BMP2 (group 5) (Figure 6(a)). PLGA/MH/BMP2-implanted group exhibited enhanced new bone formation and bony bridges at the inter-transverse, articular process area and film-implanted sites (Figure 6(a)). Based on micro-CT images, the new bone formation was evaluated by the following parameters including bone mineral density (BMD, g/cm²), percent bone volume (BV/TV, %), and trabecular thickness (Tb.Th, mm) (Figure 6(b)–(d)). The PLGA/MH/BMP2-implanted group showed significant increases in BMD, percent bone volume, and trabecular bone thickness, meaning that PLGA/MH/BMP2 could provide a more effective substrate for the promotion of bone formation.

Histological analysis

The spinal samples were decalcified for histology (Figure 7) and immunohistochemistry (Figure 8). Results of H&E staining demonstrated osteoblasts, osteocyte, and lymphocyte around the implantation site (Figure 7(a)) and revealed significant differences in average osteoblast cell counts between groups (66,585 in group 1, 102,905 in group 2, 139,897 in group 3, 321,495 in group 4, and 422,383/mm² in group 5; $p = 0.0053$) (Figure 7(b)). The average inflammatory cell count was lower in the PLGA/MH group (169,492) and the PLGA/MH/BMP2 group (151,332) compared to PLGA group (429,782), which even lower than

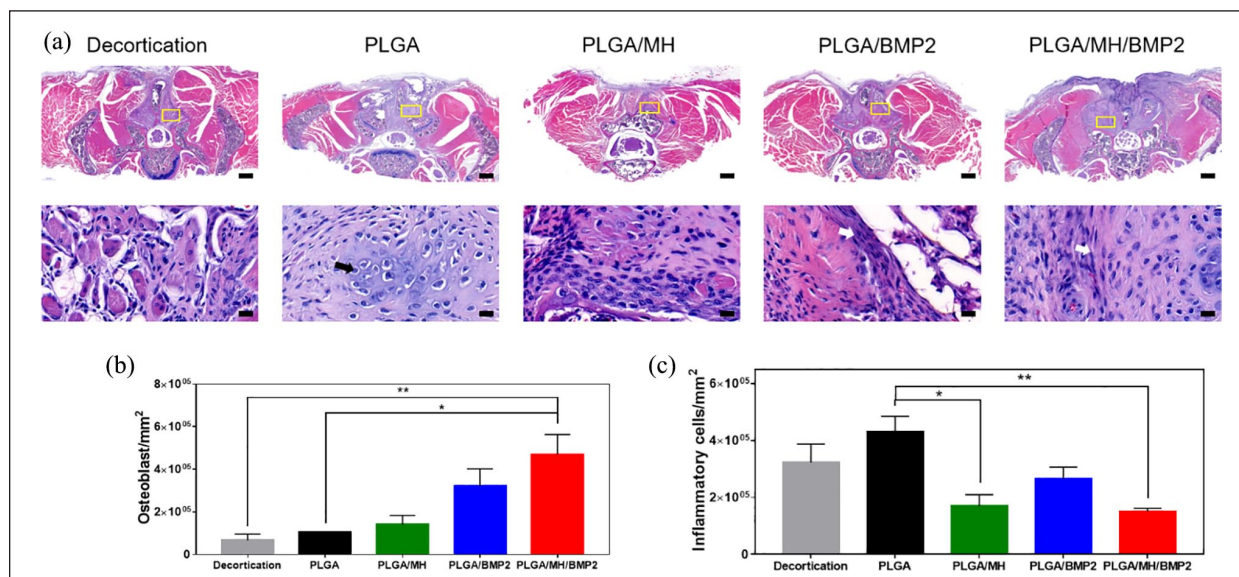


Figure 7. Hematoxylin and eosin (H&E) staining of the spine samples. (a) Representative images of H&E staining. Semi-quantification of osteoblasts (b) and inflammatory cells (c). Scale bar = 500 μm (* $p < 0.05$, ** $p < 0.01$, and *** $p < 0.001$).

group 1 (322,841/mm²). Incidentally, the average inflammatory cell count in group 3 was quite higher than in the groups that contained MH due to the acidic degradation products of PLGA (Figure 7(c)). Masson's trichrome staining (Figure 8(a)) and immunostaining for osteocalcin (Figure 8(b)) were performed to evaluate new bone formation. IL-6 immunohistochemical staining (Figure 8(c)) was carried out to confirm the inflammatory response. The PLGA/MH/BMP group showed new bone formations, which were confirmed at ROI (yellow box) using Masson's trichrome staining and highest intensity. The average immunoreactivity of osteocalcin showed statistically significant differences between the groups; the PLGA/MH/BMP group also revealed the highest osteocalcin immunoreactivity (decortication-only group: 2,195,334, PLGA group: 33,214,786, PLGA/MH group: 60,477,386, PLGA/BMP group: 52,115,659, and PLGA/MH/BMP group: 124,816,009 A.U.) (Figure 8(b)). IL-6 immunohistochemical staining indicated that the expression of IL-6, an inflammatory marker, was high in both the PLGA and PLGA/BMP groups, whereas IL-6 expression was very low in the PLGA/MH and PLGA/MH/BMP groups (Figure 8(c)). These results suggested that MH may significantly suppress inflammatory responses (414,801 in decortications group, 1,894,904 in PLGA group, 376,402 in PLGA/MH group, 1,930,988 in PLGA/BMP group, and 549,566 A.U. in PLGA/MH/BMP). PLGA/MH/BMP was the most effective combination in both the promotion of bone formation and the reduction of inflammation.

Conclusion

Numerous bone tissue engineering studies aim to mitigate problems associated with bone grafting by using degradable scaffolds.^{16,18,20,52} PLGA has become one of the most widely used bone grafting biomaterials. As mentioned previously, using PLGA as a surgical biomaterial is required to improve biocompatibility; the acidic byproducts it produces during its degradation cause an inflammatory response at the implant site.^{53,54} The primary intention of this study was to develop a method for BMP2 immobilization on the surface of PLGA to facilitate a sustained release. The PLGA/MH/BMP2 composite was able to slowly release for up to 8 weeks. Moreover, the PLGA/MH/BMP2 composite showed higher water wettability and BMP2 loading capacity by utilizing a PDA interlayer, as well as improved cumulative BMP2 release percentage due to the incorporation of MH nanoparticles. Our findings demonstrated that the BMP2-immobilized PLGA/MH composite promoted cell attachment, proliferation, and osteogenic differentiation of MC3T3-E1 cells through increased anti-inflammatory action and pH neutralization via the addition of MH. Furthermore, in our animal study, BMP2-immobilized PLGA/MH scaffolding significantly enhanced bone formation by increasing osteogenesis and suppressing inflammatory responses. Taken together, our results suggest that the BMP2-immobilized PLGA/MH scaffold could be a good candidate for enhancing bone regeneration in spinal fusion surgery.

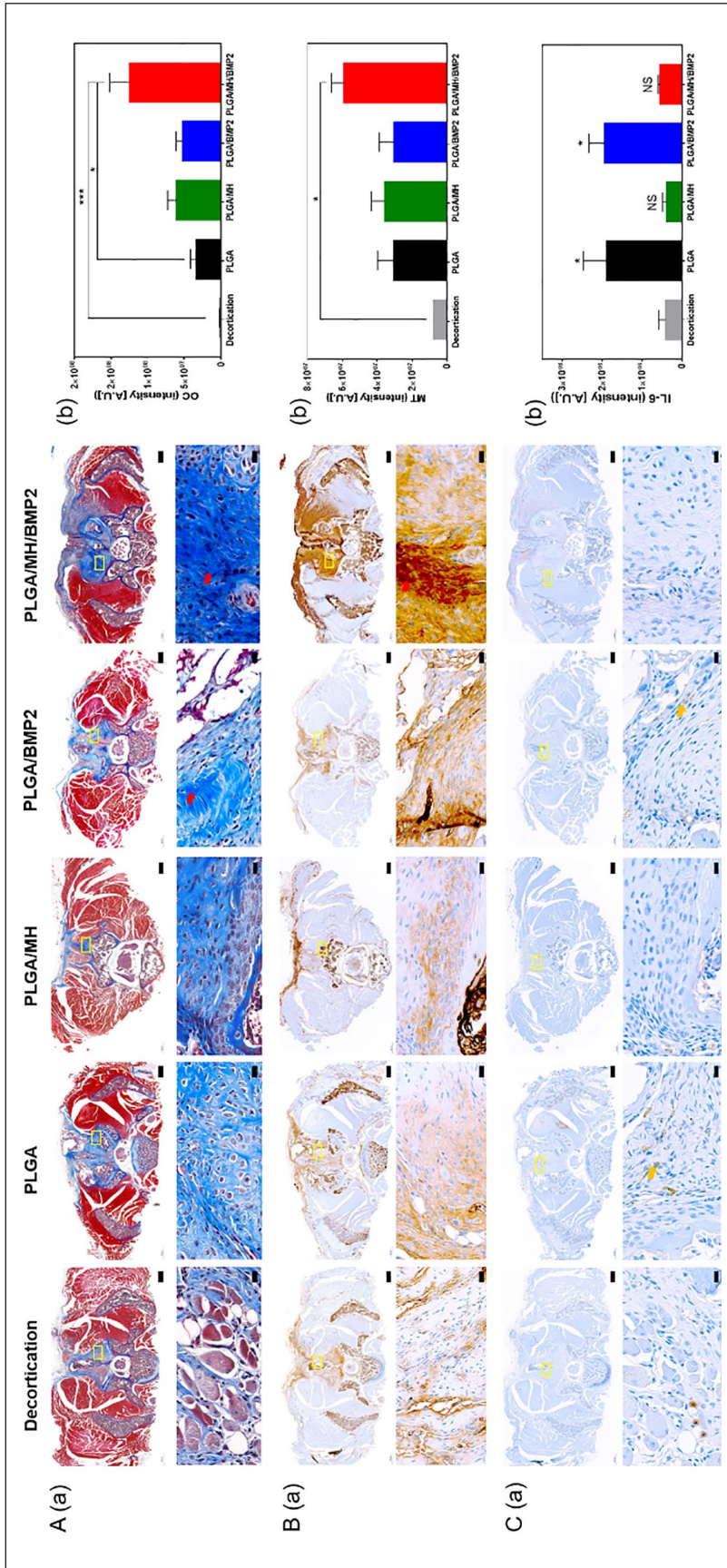


Figure 8. Masson's trichrome staining and immunohistochemistry of the spinal samples. Representative images of Masson's trichrome staining (a), immunohistochemical staining for osteocalcin (b), and IL-6 (c) with semi-quantification of Masson's trichrome staining and immunohistochemical staining for osteocalcin and IL-6 (Scale bar = 500 μ m (* $p < 0.05$, ** $p < 0.01$, and *** $p < 0.001$).

Declaration of Conflicting Interests

The author(s) declared no potential conflicts of interest with respect to the research, authorship, and/or publication of this article.

Funding

The author(s) disclosed receipt of the following financial support for the research, authorship, and/or publication of this article: This work was supported by Basic Science Research Programs (2018R1C1B508620413, 2019R1A2C1088709, and 2020R1A2B5B03002344) and Bio & Medical Technology Development Program (2018M3A9E2024579) through the National Research Foundation of Korea funded by the Ministry of Science and ICT (MSIT) and a grant of the Korea Health Technology R&D Project (HR16C0002) through the Korea Health Industry Development Institute (KHIDI), funded by the Ministry of Health & Welfare, Republic of Korea.

ORCID iDs

Da-Seul Kim  <https://orcid.org/0000-0002-6281-0434>

Hari Prasad Joshi  <https://orcid.org/0000-0002-3157-2832>

Dong Keun Han  <https://orcid.org/0000-0001-9015-9071>

Supplemental material

Additional surface analysis and *in vitro* cell assay data are available on the Supporting Information.

References

1. Benzel E, Ferrara L, Roy S, et al. Micromachines in spine surgery. *Spine* 2004; 29: 601–606.
2. Vaccaro AR, Whang PG, Patel T, et al. The safety and efficacy of OP-1 (rhBMP-7) as a replacement for iliac crest autograft for posterolateral lumbar arthrodesis: minimum 4-year follow-up of a pilot study. *Spine J* 2008; 8: 457–465.
3. Jang HJ, Park S-B, Bedair TM, et al. Effect of various shaped magnesium hydroxide particles on mechanical and biological properties of poly(lactic-co-glycolic acid) composites. *J Ind Eng Chem* 2018; 59: 266–276.
4. Fu K, Pack DW, Klivanov AM, et al. Visual evidence of acidic environment within degrading poly(lactic-co-glycolic acid) (PLGA) microspheres. *Pharm Res* 2000; 17: 100–106.
5. Casanova MR, Oliveira C, Fernandes EM, et al. Spatial immobilization of endogenous growth factors to control vascularization in bone tissue engineering. *Biomater Sci* 2020; 8: 2577–2589.
6. Rihn JA, Kirkpatrick K and Albert TJ. Graft options in posterolateral and posterior interbody lumbar fusion. *Spine (Phila Pa 1976)* 2010; 35: 1629–1639.
7. Lee JY, Lim H, Ahn JW, et al. Design of a 3D BMP-2-delivering tannylated PCL scaffold and its anti-oxidant, anti-inflammatory, and osteogenic effects in vitro. *Int J Mol Sci* 2018; 19: 3602.
8. Burova I, Wall I and Shipley RJ. Mathematical and computational models for bone tissue engineering in bioreactor systems. *J Tissue Eng* 2019; 10: 1–25.
9. Hettiaratchi MH, Krishnan L, Rouse T, et al. Heparin-mediated delivery of bone morphogenetic protein-2 improves spatial localization of bone regeneration. *Sci Adv* 2020; 6: eaay1240.
10. Park S-Y, Kim K-H, Kim S, et al. BMP-2 gene delivery-based bone regeneration in dentistry. *Pharmaceutics* 2019; 11: 393.
11. Jung SW, Oh SH, Lee IS, et al. In situ gelling hydrogel with anti-bacterial activity and bone healing property for treatment of osteomyelitis. *Tissue Eng Regen Med* 2019; 16: 479–490.
12. Zhang T, Wei Q, Fan D, et al. Improved osseointegration with rhBMP-2 intraoperatively loaded in a specifically designed 3D-printed porous Ti6Al4V vertebral implant. *Biomater Sci* 2020; 8: 1279–1289.
13. Rosenberg M, Shilo D, Galperin L, et al. Bone morphogenic protein 2-loaded porous silicon carriers for osteoinductive implants. *Pharmaceutics* 2019; 11: 602.
14. Munir A, Døskeland A, Avery SJ, et al. Efficacy of copolymer scaffolds delivering human demineralised dentine matrix for bone regeneration. *J Tissue Eng* 2019; 10: 1–16.
15. Min Q, Yu X, Liu J, et al. Chitosan-based hydrogels embedded with hyaluronic acid complex nanoparticles for controlled delivery of bone morphogenetic protein-2. *Pharmaceutics* 2019; 11: 214.
16. Hines DJ and Kaplan DL. Poly(lactic-co-glycolic) acid-controlled-release systems: experimental and modeling insights. *Crit Rev Ther Drug Carrier Syst* 2013; 30: 257–276.
17. Burova I, Peticone C, De Silva Thompson D, et al. A parameterised mathematical model to elucidate osteoblast cell growth in a phosphate-glass microcarrier culture. *J Tissue Eng* 2019; 10: 1–14.
18. Lee S-Y, Koak J-Y, Kim S-K, et al. Cellular response of anodized titanium surface by poly(lactide-co-glycolide)/bone morphogenic protein-2. *Tissue Eng Regen Med* 2018; 15: 591–599.
19. Agrawal V and Sinha M. A review on carrier systems for bone morphogenetic protein-2. *J Biomed Mater Res Part B Appl Biomater* 2017; 105: 904–925.
20. Dashnyam K, Lee J-H, Mandakhbayar N, et al. Intra-articular biomaterials-assisted delivery to treat temporomandibular joint disorders. *J Tissue Eng* 2018; 9: 1–12.
21. Woo BH, Fink BF, Page R, et al. Enhancement of bone growth by sustained delivery of recombinant human bone morphogenetic protein-2 in a polymeric matrix. *Pharm Res* 2001; 18: 1747–1753.
22. Ortega-Oller I, Padial-Molina M, Galindo-Moreno P, et al. Bone regeneration from PLGA micro-nanoparticles. *Biomed Res Int* 2015; 2015: 415289.
23. Mohamed F and van der Walle CF. Engineering biodegradable polyester particles with specific drug targeting and drug release properties. *J Pharm Sci* 2008; 97: 71–87.
24. Hollinger J, Mayer M, Buck D, et al. Poly(α -hydroxy acid) carrier for delivering recombinant human bone morphogenetic protein-2 for bone regeneration. *J Control Rel* 1996; 39: 287–304.
25. Hernández A, Reyes R, Sánchez E, et al. In vivo osteogenic response to different ratios of BMP-2 and VEGF released from a biodegradable porous system. *J Biomed Mater Res Part A* 2012; 100: 2382–2391.
26. Byrne DP, Lacroix D, Planell JA, et al. Simulation of tissue differentiation in a scaffold as a function of porosity,

- young's modulus and dissolution rate: application of mechano-biological models in tissue engineering. *Biomaterials* 2007; 28: 5544–5554.
27. Virlan MJR, Miricescu D, Totan A, et al. Current uses of poly(lactic-co-glycolic acid) in the dental field: a comprehensive review. *J Chem*. Epub ahead of print January 2015. DOI: 10.1155/2015/525832.
 28. Kim JY, Chun SY, Lee SH, et al. In vivo validation model of a novel anti-inflammatory scaffold in interleukin-10 knock-out mouse. *Tissue Eng Regen Med* 2018; 15: 381–392.
 29. Kum CH, Cho Y, Seo SH, et al. A poly(lactide) stereo-complex structure with modified magnesium oxide and its effects in enhancing the mechanical properties and suppressing inflammation. *Small* 2014; 10: 3783–3794.
 30. Lee SK, Han C-M, Park W, et al. Synergistically enhanced osteoconductivity and anti-inflammation of PLGA/ β -TCP/Mg(OH)₂ composite for orthopedic applications. *Mater Sci Eng C* 2019; 94: 65–75.
 31. Park KS, Kim BJ, Lih E, et al. Versatile effects of magnesium hydroxide nanoparticles in PLGA scaffold-mediated chondrogenesis. *Acta Biomater* 2018; 73: 204–216.
 32. Lih E, Park KW, Chun SY, et al. Biomimetic porous PLGA scaffolds incorporating decellularized extracellular matrix for kidney tissue regeneration. *ACS Appl Mater Interfaces* 2016; 8: 21145–21154.
 33. Lih E, Park W, Park KW, et al. A bioinspired scaffold with anti-inflammatory magnesium hydroxide and decellularized extracellular matrix for renal tissue regeneration. *ACS Cent Sci* 2019; 5: 458–467.
 34. Lih E, Kum CH, Park W, et al. Modified magnesium hydroxide nanoparticles inhibit the inflammatory response to biodegradable poly(lactide-co-glycolide) implants. *ACS Nano* 2018; 12: 6917–6925.
 35. Lee HW, Seo SH, Kum CH, et al. Fabrication and characteristics of anti-inflammatory magnesium hydroxide incorporated PLGA scaffolds formed with various porogen materials. *Macromol Res* 2014; 22: 210–218.
 36. Kum CH, Cho Y, Joung YK, et al. Biodegradable poly(L-lactide) composites by oligolactide-grafted magnesium hydroxide for mechanical reinforcement and reduced inflammation. *J Mater Chem B* 2013; 1: 2764–2772.
 37. Bedair TM, Bedair HM, Ko KW, et al. Persulfated flavonoids accelerated re-endothelialization and improved blood compatibility for vascular medical implants. *Colloids Surf B Biointerfaces* 2019; 181: 174–184.
 38. Zhang J, Li J, Jia G, et al. Improving osteogenesis of PLGA/HA porous scaffolds based on dual delivery of BMP-2 and IGF-1 via a polydopamine coating. *RSC Adv* 2017; 7: 56732–56742.
 39. Bedair TM, Kang SN, Joung YK, et al. A promising approach for improving the coating stability and in vivo performance of biodegradable polymer-coated sirolimus-eluting stent. *J Biomed Nanotechnol* 2016; 12: 2015–2028.
 40. Edith D and Six J-L. Surface characteristics of PLA and PLGA films. *Appl Surf Sci* 2006; 253: 2758–2764.
 41. Fu J, Chen Z, Wang M, et al. Adsorption of methylene blue by a high-efficiency adsorbent (polydopamine microspheres): kinetics, isotherm, thermodynamics and mechanism analysis. *Chem Eng J* 2015; 259: 53–61.
 42. Zhang Y, Lynge ME, Teo BM, et al. Mixed poly(dopamine)/poly(L-lysine)(composite) coatings: from assembly to interaction with endothelial cells. *Biomater Sci* 2015; 3: 1188–1196.
 43. Bhattarai SR, Bhattarai N, Viswanathamurthi P, et al. Hydrophilic nanofibrous structure of polylactide; fabrication and cell affinity. *J Biomed Mater Res Part A* 2006; 78: 247–257.
 44. Ko E, Yang K, Shin J, et al. Polydopamine-assisted osteoinductive peptide immobilization of polymer scaffolds for enhanced bone regeneration by human adipose-derived stem cells. *Biomacromolecules* 2013; 14: 3202–3213.
 45. Wei Q, Zhang F, Li J, et al. Oxidant-induced dopamine polymerization for multifunctional coatings. *Polym Chem* 2010; 1: 1430–1433.
 46. Chang Q, Cai J, Wang Y, et al. Large adipose tissue generation in a mussel-inspired bioreactor of elastic-mimetic cryogel and platelets. *J Tissue Eng* 2018; 9: 1–16.
 47. Cheng M, Deng J, Yang F, et al. Study on physical properties and nerve cell affinity of composite films from chitosan and gelatin solutions. *Biomaterials* 2003; 24: 2871–2880.
 48. Zhu X, Cui W, Li X, et al. Electrospun fibrous mats with high porosity as potential scaffolds for skin tissue engineering. *Biomacromolecules* 2008; 9: 1795–1801.
 49. Zhang S, Zhang Y, Bi G, et al. Mussel-inspired polydopamine biopolymer decorated with magnetic nanoparticles for multiple pollutants removal. *J Hazard Mater* 2014; 270: 27–34.
 50. Washington MA, Balmert SC, Fedorchak MV, et al. Monomer sequence in PLGA microparticles: effects on acidic microclimates and in vivo inflammatory response. *Acta Biomater* 2018; 65: 259–271.
 51. Janning C, Willbold E, Vogt C, et al. Magnesium hydroxide temporarily enhancing osteoblast activity and decreasing the osteoclast number in peri-implant bone remodelling. *Acta Biomater* 2010; 6: 1861–1868.
 52. Re F, Sartore L, Moulisova V, et al. 3D gelatin-chitosan hybrid hydrogels combined with human platelet lysate highly support human mesenchymal stem cell proliferation and osteogenic differentiation. *J Tissue Eng* 2019; 10: 1–16.
 53. Lendlein A and Langer R. Biodegradable, elastic shape-memory polymers for potential biomedical applications. *Science* 2002; 296: 1673–1676.
 54. Yoon SJ, Kim SH, Ha HJ, et al. Reduction of inflammatory reaction of poly(D,L-lactic-co-glycolic acid) using demineralized bone particles. *Tissue Eng Part A* 2008; 14: 539–547.